AIP | Applied Physics Letters

Slow light enhanced sensitivity of resonance modes in photonic crystal biosensors

Wei-Cheng Lai, Swapnajit Chakravarty, Yi Zou, Yunbo Guo, and Ray T. Chen

Citation: Appl. Phys. Lett. **102**, 041111 (2013); doi: 10.1063/1.4789857
View online: http://dx.doi.org/10.1063/1.4789857
View Table of Contents: http://apl.aip.org/resource/1/APPLAB/v102/i4
Published by the American Institute of Physics.

Slow light enhanced sensitivity of resonance modes in photonic crystal biosensors

Wei-Cheng Lai,[1,a)] Swapnajit Chakravarty,[2,a),b)] Yi Zou,[1] Yunbo Guo,[2] and Ray T. Chen[1,2,c)]
[1]*Department of Electrical and Computer Engineering, University of Texas at Austin, Austin, Texas 78712, USA*
[2]*Omega Optics, Inc., Austin, Texas 78759, USA*

(Received 30 September 2012; accepted 15 January 2013; published online 29 January 2013)

We demonstrate experimentally that in photonic crystal sensors with a side-coupled cavity-waveguide configuration, group velocity of the propagating mode in the coupled waveguide at the frequency of the resonant mode plays an important role in enhancing the sensitivity. In linear L13 photonic crystal microcavities, with nearly same resonance mode quality factors ~7000 in silicon-on-insulator devices, sensitivity increased from 57 nm/RIU to 66 nm/RIU as group index in the coupled waveguide increased from 10.2 to 13.2. Engineering for highest sensitivity in such planar integrated sensors, thus, requires careful slow light design for optimized sensor sensitivity. © *2013 American Institute of Physics*. [http://dx.doi.org/10.1063/1.4789857]

Over the past several years, significant research has focused on achieving higher sensitivities in chip-integrated label-free biosensors based on different methods such as ring resonator,[1] surface plasmon resonance (SPR),[2] directional coupler,[3] Mach-Zehnder interferometer (MZI),[4] and photonic crystal (PC).[5–7] Amongst all devices in integrated optics, PC devices provide the unique characteristic of slow light in photonic crystal waveguide (PCW) architectures which effectively enhances light-matter interaction,[8] thereby leading to high sensitivities in compact device geometries. The advantage of slow light has been proved in several applications such as optical modulator,[9] optical infrared absorption sensing on liquid contaminants,[10] and optical spectrometry on gaseous contaminants.[11] Highest sensitivity devices on the two-dimensional PC platform have also been demonstrated by our group as biosensors for chip-integrated microarray applications in proteomics.[7] We demonstrated methods to increase the quality factor (Q) as well as the sensitivity in PC microcavity coupled PC waveguide architectures by tailoring the radiation loss as well as the optical mode volume of PC microcavity resonances.[5,7] In this paper, we show experimentally that in a PC microcavity coupled waveguide system, the magnitude of slow light in the coupling waveguide also contributes to enhanced sensor sensitivity.

The device investigated is a L13 PC microcavity coupled to a W1 PCW in silicon in a silicon-on-insulator (SOI) platform in which we have previously demonstrated highest biosensing sensitivity among competing optical technologies at a concentration of 0.1 μg/ml.[7] The PC consists of a triangular lattice of air holes with lattice constant $a = 392$ nm. The air holes have radius $r = 0.277a$ and the height of the silicon slab is $h = 250$ nm. The W1 PCW is formed by removing a complete row of air holes along the $\Gamma-K$ direction in a triangular lattice photonic crystal. The L13 PC microcavity is formed by removing 13 air holes in dielectric silicon parallel to the W1 PCW. Fig. 1(a) inset shows a scanning electron micrograph (SEM) of the device. Light transmitted down the PCW is dropped at frequencies corresponding to the resonance frequency of the

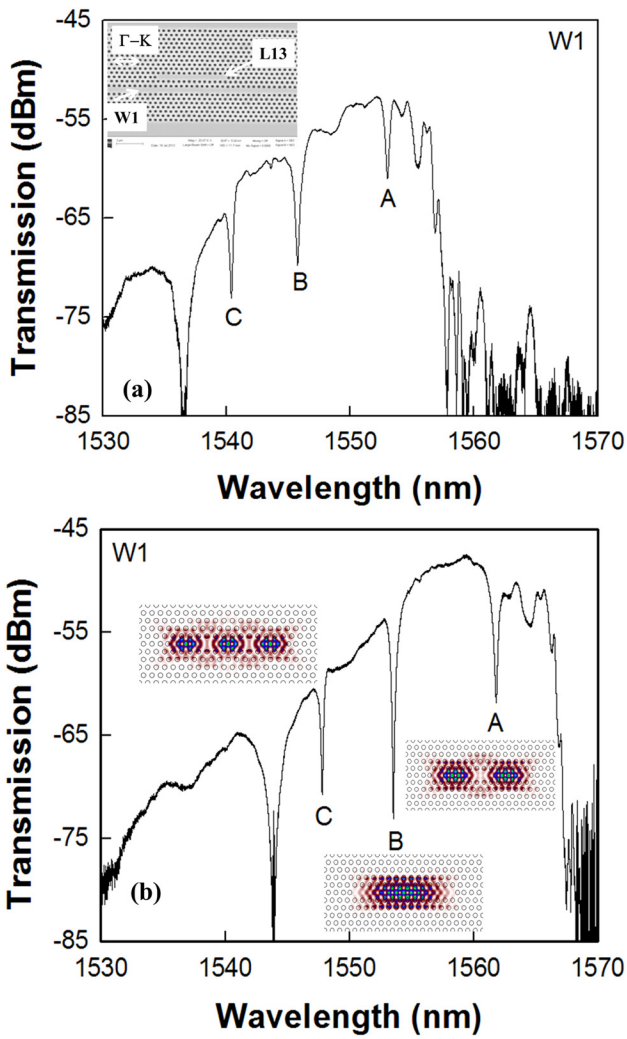

FIG. 1. Experimental transmission spectrum of device in (a) water and (b) glycerol, showing the resonance modes and mode profiles. Inset of (a) shows SEM of L13 PC microcavity and W1 waveguide.

[a)]W.-C. Lai and S. Chakravarty contributed equally to this work.
[b)]Electronic mail: swapnajit.chakravarty@omegaoptics.com.
[c)]Electronic mail: raychen@uts.cc.utexas.edu.

microcavity. A typical transmission spectrum of the L13 PC microcavity is shown in Fig. 1(a) for water and Fig. 1(b) for glycerol. The sensor works on the principle that refractive index changes in the vicinity of the PC microcavity lead to a shift in the resonance wavelength, the sensitivity of the sensor determined by the magnitude of the resonance wavelength change for a given change in refractive index in chemical sensing, or a given change in biomolecule concentration in biosensing.

Fig. 1(a) shows that multiple resonances of the L13 PC microcavity are dropped from the transmission spectrum of the W1 PCW. We limit our study to the three modes labeled A, B, and C nearest to the W1 PCW transmission band edge at 1558 nm in water in Fig. 1(a) and at 1568 nm in glycerol as in Fig. 1(b). Fig. 2(a) plots the dispersion diagram for the photonic crystal waveguide in water that shows the resonance mode of the L13 PC microcavity coupled to the W1 PCW. The resonance mode frequencies of A, B, and C are calculated from the experimental transmission spectrum in Fig. 1(a). The band edge in Fig. 1(a) corresponds approximately to $a/\lambda = 0.25$ where the simulated group index is $n_g = 33$ as seen from Fig. 2(a), obtained by three-dimensional (3D) plane-wave expansion (PWE) simulations. The experimental band edge is offset from the simulated band edge due to high transmission losses at higher n_g values and is consistent with maximum $n_g \sim 35$ observed experimentally in air-clad PCW structures.[12] It is observed that at the coupling frequencies of modes A, B, and C, the group indices of the W1 PCW guided mode are 13.2, 9.8, and 7.9, respectively. Due to the asymmetry out-of-plane of 3-D PWE simulation in water, the band edge at $a/\lambda = 0.25$ and the group index values are estimated, but very close to actual values.

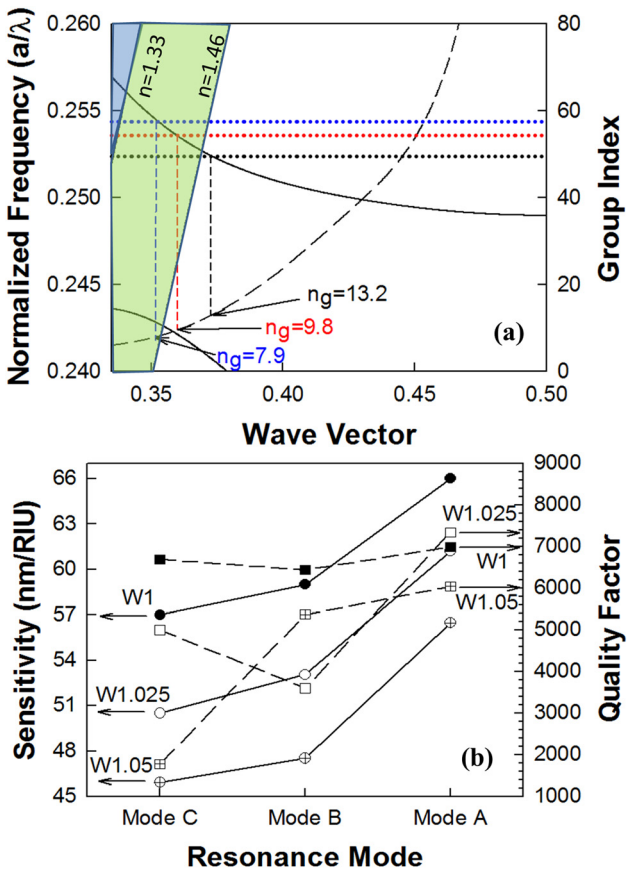

FIG. 2. (a) Dispersion diagram in water of the W1 PCW with the coupled L13 PC microcavity mode frequencies A, B, and C shown in black, red, and blue dotted lines, respectively. Simulated group index of the W1 PCW is shown on the right axis. (b) Sensitivity values and Q-factors in water of resonance modes A, B, and C are shown for W1 as filled circles and filled squares, respectively, for W1.025 as open circles and open squares and for W1.05 as crossed circle and crossed squares, respectively.

Devices were measured in water (refractive index $n = 1.33$) and glycerol ($n = 1.46$) and the bulk sensitivity in nm/RIU (RIU = refractive index unit) was determined and plotted in Fig. 2(b) for the individual modes A, B, and C. Fig. 2(b) shows that mode A has the highest bulk sensitivity of 66 nm/RIU. Fig. 2(b) also plots the Q and the bulk sensitivities of modes A, B, and C when the L13 PC microcavity is coupled to wider PCWs W1.025 and W1.05. (W1.05 indicates that the width of the PCW is $1.05 \times \sqrt{3}a$, where a is the lattice constant of the PC pattern).

Fig. 3 plots the wavelength shift of the respective modes A, B, and C as a function of concentration of the biomolecule avidin which binds to its conjugate specific biotin that is immobilized on the L13 PC microcavity that is coupled to a W1 PCW. The procedure of surface functionalization, target antibody (biotin) immobilization, and subsequent biosensing has been described in detail in Ref. 7 and is not repeated here. The surface sensitivity to biosensing is determined by the magnitude of the resonance wavelength shift when a specific concentration of probe biomolecule avidin is introduced in solution and binds to its conjugate specific biomolecule biotin. It is observed from Fig. 3 that mode A shows the highest sensitivity. The difference in wavelength shifts of the resonance modes is much larger than the 0.02 nm wavelength accuracy of our optical spectrum analyzer.

With respect to the modes A, B, and C, it is expected that the sensitivity is determined by the mode Q as well as the optical overlap of the mode with the analyte near the surface of the PC microcavity and the holes in the vicinity of the PC microcavity. The total quality factor (Q) of a resonance mode in the side-coupled cavity-waveguide architectures is given[7,13] by

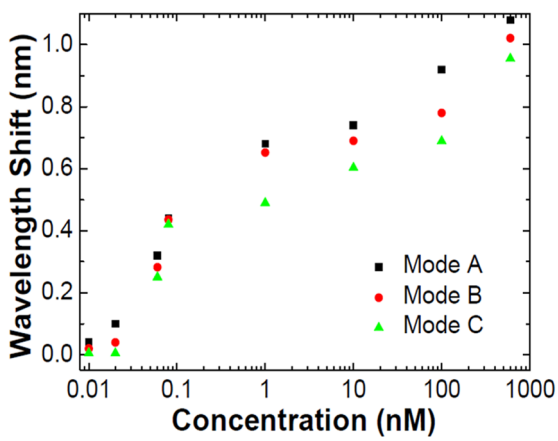

FIG. 3. The wavelength shift of each resonance modes at different concentrations. Solid square dots denote the resonance mode A. Solid circle dots denote mode B, and the solid triangle dots are mode C.

$$\frac{1}{Q} = \frac{1}{Q_i} + \frac{1}{Q_R} + \frac{1}{Q_{WG}}, \quad (1)$$

where $Q_i = \omega\tau_i, \tau_i$ denotes the intrinsic cavity loss time constant which includes surface roughness and material absorption losses, $Q_R = \omega\tau_R, \tau_R$ denotes the radiation loss time constant from the microcavity and $Q_{WG} = \omega\tau_{WG}, \tau_{WG}$ denotes the leakage loss time constant from the microcavity to the waveguide. ω denotes the resonance frequency of the PC microcavity.

$$\frac{1}{\tau_R} = \frac{P_R}{W_E}, \quad (2)$$

where P_R denotes the total power radiated by the cavity and W_E denotes the stored energy in the cavity which is proportional to the cavity mode volume.[14] We have shown previously that lower P_R and higher W_E decrease the net radiation loss rate from the cavity and hence increase the effective Q.[5,7] Higher Q results in light being trapped in the microcavity for a longer duration at the particular resonance frequency which results in enhanced light-matter interaction and thus higher sensitivity. Q of the modes A and B are nearly the same within the range of experimental variation of Q. The optical overlap of modes A and B, estimated from the mode profile by integrating over an area where the E-field intensity is more than 50% of the maximum value[15] and including the entire internal surface area of the holes along the periphery of the PC microcavity, is nearly the same. However, the optical coupling efficiency from the W1 PCW of resonance mode A is much higher than that of B. The coupling efficiency η between the cavity and the waveguide is described by[16]

$$\eta \propto \frac{1}{v_g}, \quad (3)$$

where v_g denotes the group velocity at the resonance frequency of the corresponding optical mode. v_g is inversely proportional to n_g. Since the coupling strength is inversely proportional to v_g, farther away from the band edge where v_g is high, the coupling strength is low. As a result of the lower optical coupling of incident light into the optical cavity for mode B compared to mode A, light-matter interaction inside the cavity is also reduced which contributes to the lower sensitivity of B compared to A. Similarly, resonance modes A, B, and C have decreasing sensitivity in order, when the L13 PC microcavity is coupled to the wider PCWs W1.025 and W1.05. We also note from Fig. 2(a) that the PCW mode is leaky (above the light line for the silicon dioxide lower cladding) at the coupling frequencies of modes B and C but non-leaky for mode A. The leaky behavior would lead to higher optical power coupling into the mode A compared to modes B and C, independent of the group index value, that may also result in higher sensitivity of mode A compared to modes B and C.

In order to separate the effects of Q_R and Q_{WG}, and also the contribution from the leaky behavior of the waveguide modes, the coupling of the resonance mode A to the PCW is studied at different propagation group velocities of the PCW. Fig. 4(a) shows the dispersion diagrams of the W1, W1.025, and W1.05 PCWs in water. The coupling frequency of the L13 resonance mode is shown. The mode A moves to lower frequencies with increased width of the PCW due to increased dielectric fraction in the vicinity of the L13 PC microcavity. The waveguide mode is non-leaky (below the light line for the silicon dioxide lower cladding) for all coupling conditions of mode A. The simulated group index values at the coupling frequencies are indicated in Fig. 4(a). The group indices of the W1, W1.025, and W1.05 PCW at the coupling frequency of the resonance mode A of the L13 PCW are 13.2, 12.7, and 10.2, respectively. Figs. 4(b) and 4(c) show the experimental transmission spectra of W1.025 and W1.05 PCWs in water.

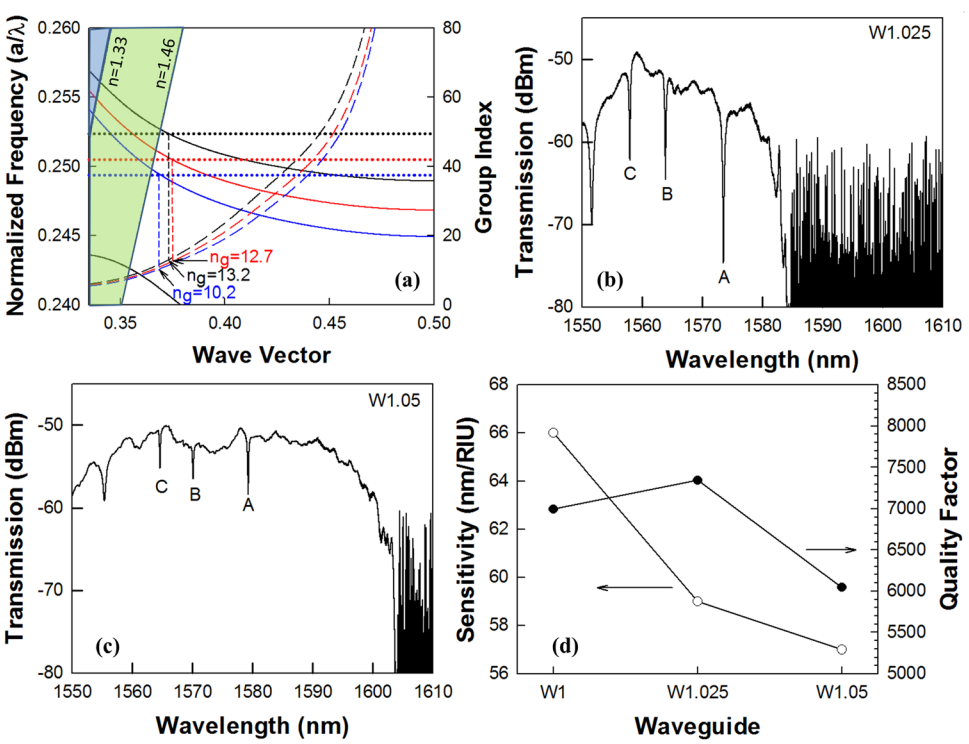

FIG. 4. (a) Dispersion diagrams of W1 (black), W1.025 (red), and W1.05 (blue) PCWs with coupled L13 PC microcavity in water. Resonant mode A in each case is indicated by dotted lines. Group index is plotted and magnitude at the coupling frequency indicated in respective colors (b) W1.025 and (c) W1.05 PCW experimental transmission spectra with coupled L13 PC microcavity. (d) Q-factor in water and bulk sensitivity comparison of resonance mode A in each PCW in (a).

Fig. 4(d) shows the results of the sensing experiments for the three waveguides with coupled L13 PC microcavity resonance A, when the device is measured in water and glycerol. In an uncoupled cavity, Q_R of the resonance mode A would increase from W1 to W1.05 due to the reduced radiation loss P_R, as the mode moves towards the dielectric band in the band diagram. Q_i can also be expected to increase from W1 to W1.05 due to reduced roughness scattering from the air holes on the side of the W1 PCW opposite to that of the PC microcavity, as the PC microcavity moves farther away from the W1 PCW. Furthermore, from Fig. 1(b), we note that the optical mode overlap of the resonance modes A with the analyte primarily occurs in the first two rows of holes along the periphery of the L13 PC microcavity which is unchanged from W1 to W1.025 and W1.05 since the L13 PC microcavity is located two periods away from the PCW in each case. At the coupling frequency of the resonance mode A, the PCW mode is non-leaky. Hence, the additional factor that results in higher sensitivity of resonance mode A in W1 compared to W1.05 PCW is η and thus v_g.

As expected from Eq. (3), a lower v_g leads to higher coupling efficiency of light from the W1 PCW to the L13 PC microcavity resonance mode A, leading to more light-matter interaction in the case of the W1 PCW versus the W1.05 PCW. Similarly, the sensitivity of the resonant mode A for the W1 PCW is higher than in the W1.025 PCW, as observed from Fig. 4(d), due to the higher group index of W1 at the coupling frequency of the L13 PC microcavity resonance A. Previously, we have shown that increased Q_R increases device sensitivity.[7] The control experiments confirm that, in addition to Q and the optical mode overlap with analyte, slow group velocities of light propagating in the PCW contribute to the enhanced light-matter interaction and thus the enhanced sensitivities of resonance modes in PC microcavities. Similar trends are observed for modes B and C from Fig. 2(b)

Of course, a higher η leads to lower Q_{WG}. A lower Q_{WG} would reduce the effective Q, which would reduce the sensitivity to detect small changes in concentrations due to the broader linewidth of the resonance mode. Hence, methods to improve Q_{WG} include moving the resonance cavity farther away from the W1 PCW while at the same time, balancing the sensitivity to arrive at an optimized design with maximum slow light contribution. We also note that increasing slow light contribution to the sensitivity also requires that slow light engineering minimizing reflection losses be performed at the input and output interfaces of the PCW with ridge waveguides for high signal-to-noise ratio in measurements as we have demonstrated earlier.[7]

In summary, we demonstrated that in side coupled PC cavity-waveguide sensors, in addition to the Q of the uncoupled PC microcavity and the optical mode overlap with analyte, slow light in the coupled PCW also contributes to the enhanced sensitivities of resonance modes.

The authors acknowledge the National Cancer Institute for supporting this work under the SBIR program (Contract Nos. HHSN261201000085C and HHSN261201200043C). W.C.L., Y.Z., and R.T.C. also acknowledge AFOSR MURI (Contract No. FA9550-08-1-0394).

[1]M. Iqbal, M. A. Gleeson, B. Spaugh, F. Tybor, W. G. Gunn, M. Hochberg, T. Baehr-jones, R. C. Bailey, and L. C. Gunn, IEEE J. Sel. Top. Quantum Electron. **16**, 654 (2010).
[2]H. Sípová, S. Zhang, A. M. Dudley, D. Galas, K. Wang, and J. Homola, Anal. Chem. **82**, 10110 (2010).
[3]V. M. N. Passaro, F. Dell'olio, C. Ciminelli, and M. N. Armenise, Sensors **9**, 1012 (2009).
[4]A. Densmore, M. Vachon, D.-X. Xu, S. Janz, R. Ma, Y.-H. Li, G. Lopinski, A. Delâge, J. Lapointe, C. C. Luebbert, Q. Y. Liu, P. Cheben, and J. H. Schmid, Opt. Lett. **34**, 3598 (2009).
[5]W.-C. Lai, S. Chakravarty, Y. Zou, and R. T. Chen, Opt. Lett. **37**, 1208 (2012).
[6]Y. Zou, S. Chakravarty, W.-C. Lai, C.-Y. Lin, and R. T. Chen, Lab Chip **12**, 2309 (2012).
[7]S. Chakravarty, Y. Zou, W.-C. Lai, and R. T. Chen, Biosens. Bioelectron. **38**, 170 (2012).
[8]T. F. Krauss, J. Phys. D: Appl. Phys. **40**, 2666 (2007).
[9]X. Wang, C.-Y. Lin, S. Chakravarty, J. Luo, A. K.-Y. Jen, and R. T. Chen, Opt. Lett. **36**, 882 (2011).
[10]W.-C. Lai, S. Chakravarty, X. Wang, C. Lin, and R. T. Chen, Opt. Lett. **36**, 984 (2011).
[11]W.-C. Lai, S. Chakravarty, X. Wang, C. Lin, and R. T. Chen, Appl. Phys. Lett. **98**, 023304 (2011).
[12]S. Rahimi, A. Hosseini, X. Xu, H. Subbaraman, and R. T. Chen, Opt. Express **19**, 21832 (2011).
[13]A. Faraon, E. Waks, D. Englund, I. Fushman, and J. Vuckovic, Appl. Phys. Lett. **90**, 073102 (2007).
[14]J. Vuckovic, M. Loncar, H. Mabuchi, and A. Scherer, IEEE J. Quantum Electron. **38**(7), 850 (2002).
[15]K. Nagahara, M. Morifuji, and M. Kondow, Photonics Nanostruct. Fundam. Appl. **9**, 261 (2011).
[16]D. Dorfner, T. Zabel, T. Hürlimann, N. Hauke, L. Frandsen, U. Rant, G. Abstreiter, and J. Finley, Biosens. Bioelectron. **24**, 3688 (2009).